P2mip

NASA TECHNICAL MEMORANDUM

NASA TM X-71548

NASA TM X-71548

REYNOLDS NUMBER EFFECTS ON BOATTAIL DRAG OF EXHAUST NOZZLES FROM WIND TUNNEL AND FLIGHT TESTS

by Fred A. Wilcox, and Roger Chamberlin
Lewis Research Center
Cleveland, Ohio 44135

TECHNICAL PAPER proposed for presentation at
AGARD Fluid Dynamics Panel Specialists Meeting on
Airframe/Propulsion Interference
Rome, Italy, September 3-6, 1974

REYNOLDS NUMBER EFFECTS ON BOATTAIL DRAG OF EXHAUST NOZZLES FROM WIND TUNNEL AND FLIGHT TESTS

Fred A. Wilcox
Head, Flight Systems Section

Roger Chamberlin
Aerospace Engineer

Lewis Research Center
National Aeronautics and Space Administration
Cleveland, Ohio, U.S.A. 44135

SUMMARY

A family of nacelle mounted high angle boattail nozzles was tested to investigate Reynolds number effects on drag. The nozzles were flown on a modified F-106B and mounted on scale models of an F-106 in a wind tunnel. A 19- to 1-range of Reynolds number was covered as a result of the large size differences between models and by flying over a range of altitude. In flight the nozzles were mounted behind J-85 turbojet engines. Jet boundary simulators and a powered turbojet engine simulator were used on the wind tunnel models. Data were taken at Mach numbers of 0.6 and 0.9. Boattail drag was found to be affected by Reynolds number. The effect is a complex relationship dependent upon boundary layer thickness and nozzle boattail shape. As Reynolds number was increased from the lowest values obtained with scale models, boattail drag first increased to a maximum at the lowest flight Reynolds number and then decreased.

E-7753

SYMBOLS

A_{bt} boattail projected area

A_{max} nacelle cross-sectional area at boattail juncture

C_D boattail pressure drag coefficient, $\dfrac{\int (p - p_o) A_{bt}}{0.7\, p_o\, A_{max}\, M_o^2}$

C_p pressure coefficient, $\dfrac{p - p_o}{0.7\, p_o\, M_o^2}$

D nacelle diameter at boattail juncture

L nozzle length

M_o free-stream Mach number

P total pressure at nozzle throat

p boattail static pressure

p_o free-stream static pressure

Re Reynolds number - based on a characteristic length of 5.18 m for flight and appropriately scaled values for the wind tunnel models

X axial distance from beginning of boattail shoulder

α angle of attack

β boattail terminal angle

INTRODUCTION

Developing a working technique to predict in-flight aerodynamic performance of aircraft components has been a goal of aerodynamicists for many years. To date analytical techniques are not sufficiently developed to handle complex geometries of new aircraft. As a result the best technique available is testing small subscale models in wind tunnels. Wind tunnel testing is limited to small models, especially at transonic Mach numbers where blockage effects are critical. Because of the small size of the models, even variable density wind tunnels cannot achieve flight values of Reynolds number.

It has been found that on certain aircraft components, Reynolds number has an unpredictable effect on the aerodynamic performance. In particular, the aerodynamic drag of boattail nozzles has been found to be thus affected.

Aircraft powered by afterburning turbofan engines require large nozzle exit area variations. In a subsonic cruise condition with the engine in a nonafterburning mode, large projected boattail areas result. In order to keep the nozzle reasonably short, high boattail angles become necessary. The drag of these nozzles can be a significant percentage of total airplane drag. Sensitivity of this drag to Reynolds number introduces a large uncertainty in prediction of aircraft performance.

A family of boattail nozzles was tested, both in flight and in a wind tunnel, over a 19-to-1 range of Reynolds number. The results were previously reported in references 1 through 4. Flight tests were made using an F-106B aircraft modified to carry two underwing research nacelles. These nacelles housed J-85 engines and were 63.5 cm in diameter at the nozzles. Reynolds number was varied by flying at altitudes ranging from 3048 to 13 700 meters at subsonic speeds. The nozzles tested had several boattail geometries that displayed a wide range of sensitivity to Reynolds number. Some of the nozzles were also tested in

the Lewis Research Center 8- by 6-Foot Supersonic Wind Tunnel on 5 and 22 percent scale F-106 models (ref. 2) which provided data at the lower Reynolds numbers.

Initial results from the flight program (refs. 1 and 2), showed a trend of decreasing boattail drag for all the nozzles with increasing Reynolds number. The model data did not follow that trend. At the lower wind tunnel Reynolds numbers boattail drag decreased with decreasing Reynolds number. These drag variations with Reynolds number appeared to be a result of changes in boundary layer thickness and changes in the separated flow on the aft boattail.

A second independent investigation (ref. 5) showed the same trend at the lower Reynolds numbers. In that test, boundary layer over nozzle boattails was artificially thickened by an upstream fence to simulate operation at a lower Reynolds number.

In this paper some of the effects of nozzle boattail shape on drag variation with Reynolds number will be discussed.

APPARATUS AND PROCEDURE

Modifications to Aircraft

An F-106B (two-seat version) has been modified to carry two underwing research nacelles located symmetrically at the 32 percent semi-span position (fig. 1). The elevons were cut out over the nacelles and replaced by a fixed section. The nacelles were mounted to the wing by means of forward and rear links which allowed axial forces to be measured by a load cell (fig. 2). Drag data presented herein, however, were obtained by integration of pressure measurements on the boattail surfaces. Normal shock inlets were used in the flights described. The nacelles were mounted with a negative incidence of $4\frac{1}{2}^{\circ}$ (relative to the wing chord) so that the aft portion of the nacelle was tangent to the wing lower surface. The nacelles housed J-85 afterburning turbojet engines. However, the tests described were restricted to nonafterburning. Secondary air to cool the engine was bled from the inlet through an adjustable valve. The nacelle and exhaust nozzles were 63.5 cm in diameter with a bulged fairing over the engine accessories.

Data were recorded in flight using the digital system described in reference 6. This system used 10 scani valves with a total capability of measuring 480 pressures. Ninety-six other parameters such as flight conditions, voltages, and temperatures could also be recorded. Data system scan time was 11.6 seconds.

Data could be taken simultaneously on left and right nozzles. Each nozzle had 10 rows of area weighted static pressure orifices, 9 in each row, which can be seen in figure 3. Also shown is a window in the tail through which movies of tufts mounted on the nozzles could be taken. A second window was located on the opposite side of the tail permitting photographs to be taken of either the left or right sides.

Flight Procedures

Research flights have been made with the modified aircraft at Mach numbers to 1.3. The flights described herein, however, were made at Mach numbers from 0.6 to 0.9, and altitudes to 13 700 m. In order to vary Reynolds number while holding Mach number and angle of attack constant, most of the data were recorded while in coordinated turns. Flights at the lowest altitudes (3048 m) were made in turns of highest load factor; about 2.5 g. Data at 13 700 m altitude was obtained in level flight. Thus, the high angle of attack required to sustain level flight at high altitude was also obtained at low altitude. The Reynolds number was based on a characteristic length of 5.18 m which takes into consideration the wing chord at the nacelle station (7.32 m) and the nacelle length (3.96 m).

Wind Tunnel Models

Figure 4 shows the 5 percent scale F-106 model that was tested in the Lewis Research Center 8- by 6-Foot Supersonic Wind Tunnel. This model is shown in the photograph with flow through nacelles and solid jet boundary simulators. The data presented were obtained with conical forebodies closing the inlets. Nozzles on this model had 4 rows of 8 area weighted static pressure orifices along the boattails. Data were obtained on this model at Mach numbers of 0.6 and 0.9 at angle of attack up to 15°.

The 22 percent scale half span F-106 model is shown in figure 5 mounted in the 8- by 6-Foot Supersonic Wind Tunnel. It was tested with both a turbojet engine simulator and with a conical forebody closing the inlet and a solid jet boundary simulator on the nozzle. The engine simulator incorporated a 6-stage, axial-flow compressor powered by a 3-stage, axial-flow turbine. High pressure warm air was used to drive the turbine. Details of the turbojet simulator are given in reference 7. The design characteristics of this simulator permitted independent operation over a wide range of both inlet mass flow ratio and nozzle pressure ratio which equaled those in flight.

Reynolds numbers for the models were based on scaled values of the characteristic length used for flight data. Reynolds numbers between 3.5 and 4 million were obtained for the 5 percent model and between 14.5 and 18 million for the 22 percent model.

Boattail Nozzles

Nozzles used in this program were typical of those used on military aircraft having supersonic dash capability and powered by afterburning turbofan engines. They were of three types as shown on figure 6; circular arc-conic, circular arc, and contoured. A numbering system was used to designate the various nozzles. The first two or three digits correspond to the radius ratio multiplied by 100. The last two digits correspond to the terminal boattail angle. The radius ratio is defined as the ratio of the radius of the boattail shoulder to the radius of a complete circular arc boattail with the same projected area and terminal boattail angle. Table I indicates which nozzles were tested on the two models.

All of the nozzles were flight tested. Three of the circular arc-conic boattails had a radius ratio of 0.25, one having a 16° boattail angle and the other two a 24° terminal angle. The second two had identical boattails but one was spaced 25.4 centimeters (0.4 nozzle diameters), further downstream of the wing trailing edge (designation Ex).

There was one 0.65 radius ratio circular arc-conic nozzle with a 24° trailing edge angle; one 24° circular arc nozzle and a contoured nozzle. Dimensions of the contoured nozzle are given in references 3 and 4. It was shaped to have a gradual initial turn followed by a steep turn with a maximum local angle of 31° and a reflex at the trailing edge. Photographs of these nozzles mounted on the aircraft are shown in figure 7. Tufts can be seen on some of the nozzles. The most satisfactory tuft length used is shown in figure 7(g) on the contoured nozzle.

RESULTS AND DISCUSSION

By comparing boattail drag data for the same nozzle at 5 percent, 22 percent, and full-scale, a wide range of Reynolds number could be covered. The 22 percent model was tested with an engine simulator and also with the inlets faired over and solid jet boundary simulators to determine whether data from the 5 percent model could be compared with flight data. The data of figure 8 indicate that nozzle drag is the same for both methods. In addition, the effect of nozzle pressure ratio on boattail drag is relatively small for the range of nozzle pressure ratio investigated.

The 5 percent model was used to determine the sensitivity of boattail drag to angle of attack, since some variation in angle of attack was obtained with the airplane. The effect of angle of attack was found to be small at Mach 0.6 (fig. 9) but became larger at high angles (above approximately 8°), at Mach 0.9. The sensitivity of drag to angle of attack was low at both Mach numbers for the angles obtained in flight.

The trend of boattail drag with Reynolds number is shown in figure 10 for the circular-arc-conic nozzles for both Mach numbers of 0.6 and 0.9. Drag coefficient was maximum at a value near the low end of the flight Reynolds number range and dropped off as Reynolds number was either raised or lowered. Very low values of drag coefficient were obtained with the 5 percent model. Values of drag coefficient for the 22 percent model fell in place between those of the smaller model and those from flight. In the flight range highest drag was obtained with nozzle 2524 Ex which was extended rearward out of the wing flow field. Lowest drag was obtained with the 16° nozzle 2516. The trend with all the nozzles in flight was decreasing drag with increasing Reynolds number.

The observed drag variation with Reynolds number is probably a result of changes in the boundary layer thickness and changes in the separated flow on the aft part of the boattail. Pressure distributions on a typical nozzle boattail are shown schematically in figure 11 for three values of Reynolds number. The solid lines are typical of the observed pressure distributions. The dashed lines represent the pressure distribution for inviscid flow. Drag is low at the very high Reynolds numbers. Due to thin boundary layer, the flow remains attached over all, or a major portion, of the boattail. This results in a large expansion at the boattail shoulder but allows the flow to recompress to relatively high pressures on the aft boattail, which offset the low pressures at the shoulder. As the Reynolds number is decreased the boundary layer becomes thicker. With the thicker boundary layer the flow cannot traverse the adverse pressure gradient as far and will separate sooner. As the separation on the aft boattail increases, the recompression is lost and drag increases. As the Reynolds number is lowered still further the flow at the boattail shoulder begins to change. The boundary layer becomes thicker causing separation to occur closer to the boattail shoulder which decreases the overexpansion. Eventually the beneficial effects of increasing pressure at the shoulder become large enough to offset the adverse effects of increased separation on the back of the boattail. Drag thus reaches a peak and then begins to decrease with further lowering of Reynolds number.

The usefulness of tufts as an indication of flow separation is illustrated in figure 12. Data are shown from four rows of pressure orifices with adjacent rows of tufts on the upper portion of one of the nozzles. An initial examination of the pressure curves shows that they are similar without a clear indication as to whether the flow is attached or separated. However, the last three tufts on the A and B rows indicate separated flow, while all of the tufts on rows C indicate attached flow. A close examination of the pressure curves reveals small differences in the level and shape of the No. 1 and 2 pressure rows which correspond to the separated condition. However, these differences are so small that they could not be used alone to predict separation. Unpublished data taken with dynamic pressure transducers located in a rake near the end of the 2524 boattail verified that the flow was unsteady and thus might be oscillating between attached and separated. Lag in the steady state pressure instrumentation would then produce values intermediate between the two flow conditions, similar to that of rows No. 1 and 2.

The effect of nozzle boattail shape on drag variation with Reynolds number is illustrated in figure 13. Data are shown for one of the circular arc-conic nozzles, the circular arc and the contoured nozzle at a Mach number of 0.9. The 6524 circular arc-conic nozzle was selected since it had the lowest drag at high Reynolds number, at this Mach number, of the high angled nozzles and was similar in length to the contoured nozzle. The circular arc and contoured nozzles had nearly the same low sensitivity to Reynolds number in the flight range. These two nozzles had nearly identical variation of drag with Reynolds number, with two very different boattail flow fields. The circular arc-conic nozzle drag was more sensitive to Reynolds number. Drag for this nozzle was higher than for the other two at intermediate and low Reynolds numbers.

Pressure distributions showing the reasons for these drag variations are given in figure 14 at three Reynolds numbers. Data are presented as a function of percent of boattail projected area to permit a more direct comparison of the various length nozzles. The circular arc-conic and contoured nozzles were nearly the same length and the circular arc nozzle was about 22 percent longer. At the highest flight Reynolds number (fig. 14(a)) the circular arc-conic nozzle had the most overexpansion followed by a rapid recompression and a small amount of separation beginning at about 80 percent of the projected area.

The pressure distributions for the circular arc and contoured nozzles show different types of flow.

With the circular arc nozzle attached flow was maintained over the entire boattail. Because turning is gradual with this nozzle, the expansion at the shoulder was small and the flow had a slow but continuous compression over the remainder of the boattail. The contoured nozzle also had a gradual turn at the shoulder with a relatively small expansion. However, downstream of this point the turning increased rapidly. A rapid recompression ensued followed by separation over about half the boattail projected area. The advantage of this nozzle is the minimum expansion at the shoulder and the fact that the flow compressed to a high value before it separated.

At the lowest Reynolds number obtained in flight (fig. 14(b)) the pressure distribution for the circular arc-conic nozzle showed the greatest change from that at the highest Reynolds number. There was less overexpansion at the shoulder, a less rapid recompression and more flow separation. This accounted for its increase in drag. The circular arc nozzle, because of its gradual turn, maintained an attached flow over most of the boattail and therefore had little change in boattail drag. The contoured nozzle, on the other hand, because of its rapid turning fixes the separation point and the flow remained separated over the same portion of the boattail resulting in little or no change in boattail drag.

At the much lower Reynolds number of the 5 percent scale model (fig. 14(c)), overexpansion at the shoulder was less for all nozzles. Recompression occurred more rapidly and pressures on the aft portion were generally higher than for the higher Reynolds numbers. The result was the low drag for all three nozzles shown in figure 13.

Analytical Prediction

The complex nature of flow over boattail nozzles has thus far precluded the generation of a completely satisfactory analytical model. Presz (ref. 8) has reported success in predicting the point of separation and pressure distribution on boattail nozzles. Variations in boattail pressure distributions reported in this reference are similar to those observed on the F-106 aircraft. More analysis is needed; in particular to include 3-dimensional effects.

CONCLUSIONS

A family of nacelle mounted, high angle boattail nozzles was tested to determine Reynolds number effects on drag. A 19 to 1 range of Reynolds number was covered by using nozzles mounted behind J85 turbojet engines on a modified F-106B in flight and scale models in a wind tunnel. Data were obtained at Mach numbers of 0.6 and 0.9. The following conclusions can be made:

1. Boattail drag can be strongly affected by Reynolds number. The effect is a complex relationship resulting from the effect of boundary layer characteristics on aft boattail separation.

2. As Reynolds number was increased from the lowest values for scale models, boattail drag first increased and then decreased in the range of Reynolds number obtained at full scale in flight. As a result, data from small scale models generally underpredicted full-scale drag.

3. Sensitivity of boattail drag to Reynolds number was dependent on boattail shape.

4. A contoured nozzle having a large region of separated flow had drag as low as a longer circular arc nozzle which had little flow separation. The drag sensitivity to Reynolds number was about the same as for the circular arc nozzle.

REFERENCES

1. R. Chamberlin, "Flight Investigation of 24° Boattail Nozzle Drag at Varying Subsonic Flight Conditions" - NASA TM X-2626, 1972.

2. R. Chamberlin and B. J. Blaha, "Flight and Wind Tunnel Investigation of the Effects of Reynolds Number on Installed Boattail Drag at Subsonic Speeds," AIAA Paper 73-139, AIAA/Aerospace Sciences Meeting, 11th, January 1973.

3. F. A. Wilcox, "Comparison of Ground and Flight Test Results Using a Modified F-106B Aircraft," AIAA Paper 73-1305, AIAA/SAE Propulsion Conference, 9th, November 1973.

4. R. Chamberlin, "Flight Investigation of Reynolds Number Effects on a Contoured Boattail Nozzle at Subsonic Speeds" - NASA TM X-3053, 1974.

5. D. E. Reubush and C. E. Mercer, "Exhaust Nozzle Characteristics for a Twin Jet Variable Wing Sweep Fighter Airplane Model at Mach Numbers to 2.2" - NASA TM X-2947, 1974.

6. H. W. Groth, N. E. Samanich, and P. Z. Blumenthal, "Inflight Thrust Measuring System for Underwing Nacelles Installed on a Modified F-106 Aircraft" - NASA TM X-2356, 1971.

7. F. W. Steffen, E. A. Satmary, M. R. Vanco, and S. M. Nosek, "A Turbojet Simulator for Mach Numbers up to 2.0," ASME Paper 72GT89, ASME/Gas Turbine and Fluids Engineering Conference and Product Show, March 1972.

8. W. M. Presz, Jr. and E. T. Pitkin, "Flow Separation Over Axisymmetric Afterbody Models," AIAA Paper 74-17, AIAA/Aerospace Sciences Meeting, 12th, January-February 1974.

TABLE I. - BOATTAIL NOZZLES TESTED

Type	Designation	Projected area ratio, A_{bt}/A_{max}	Length, L/D	Nozzle tested on		
				F-106	5% model	22% model
Circular arc-conic	2516	0.75	2.20	X	X	X
	2524	0.75	1.43	X	X	X
	2524 Ex	0.75	1.43	X		
	6524	0.75	1.92	X	X	X
Circular arc	10024	0.75	2.35	X	X	
Contoured		0.71	1.94	X	X	

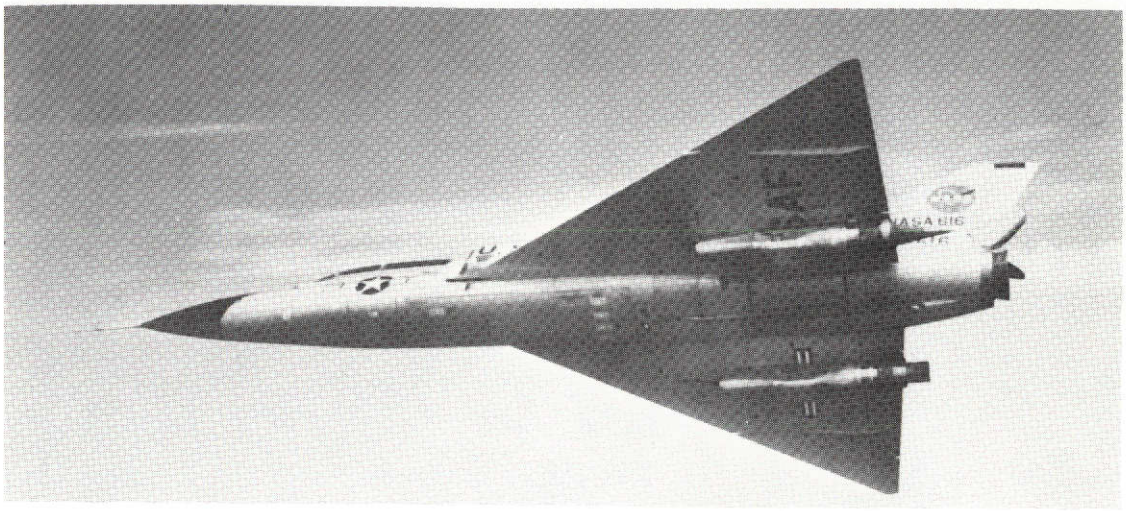

C-69-2871

Figure 1. - Modified F-106B in flight.

E-7763

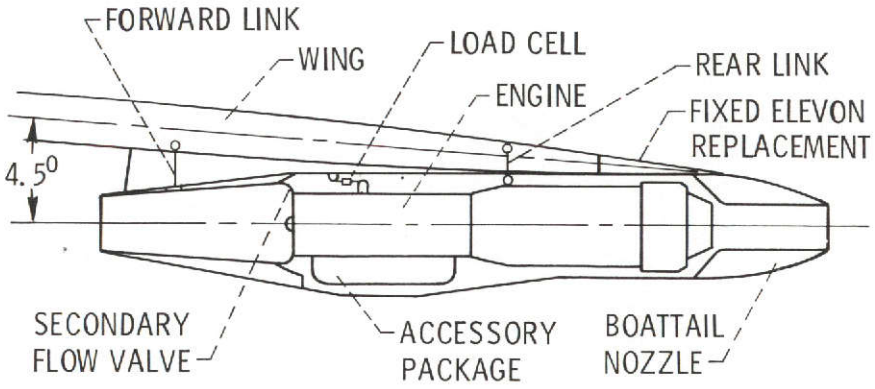

Figure 2. - Nacelle-engine installation.

Figure 3. - Boattail nozzles installed on F-106B aircraft.

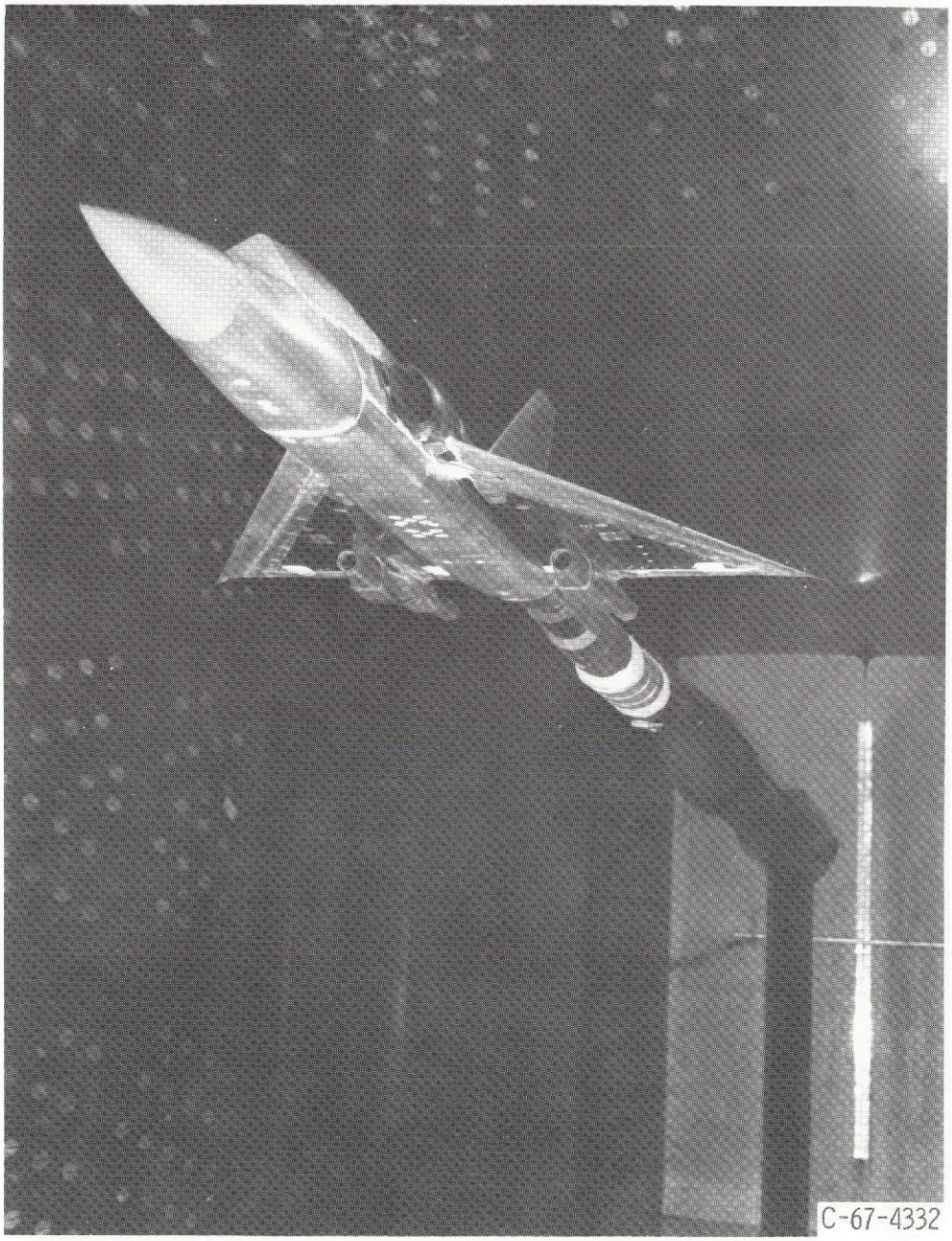

Figure 4. - 0.05 scale F-106 model in 8x6 tunnel.

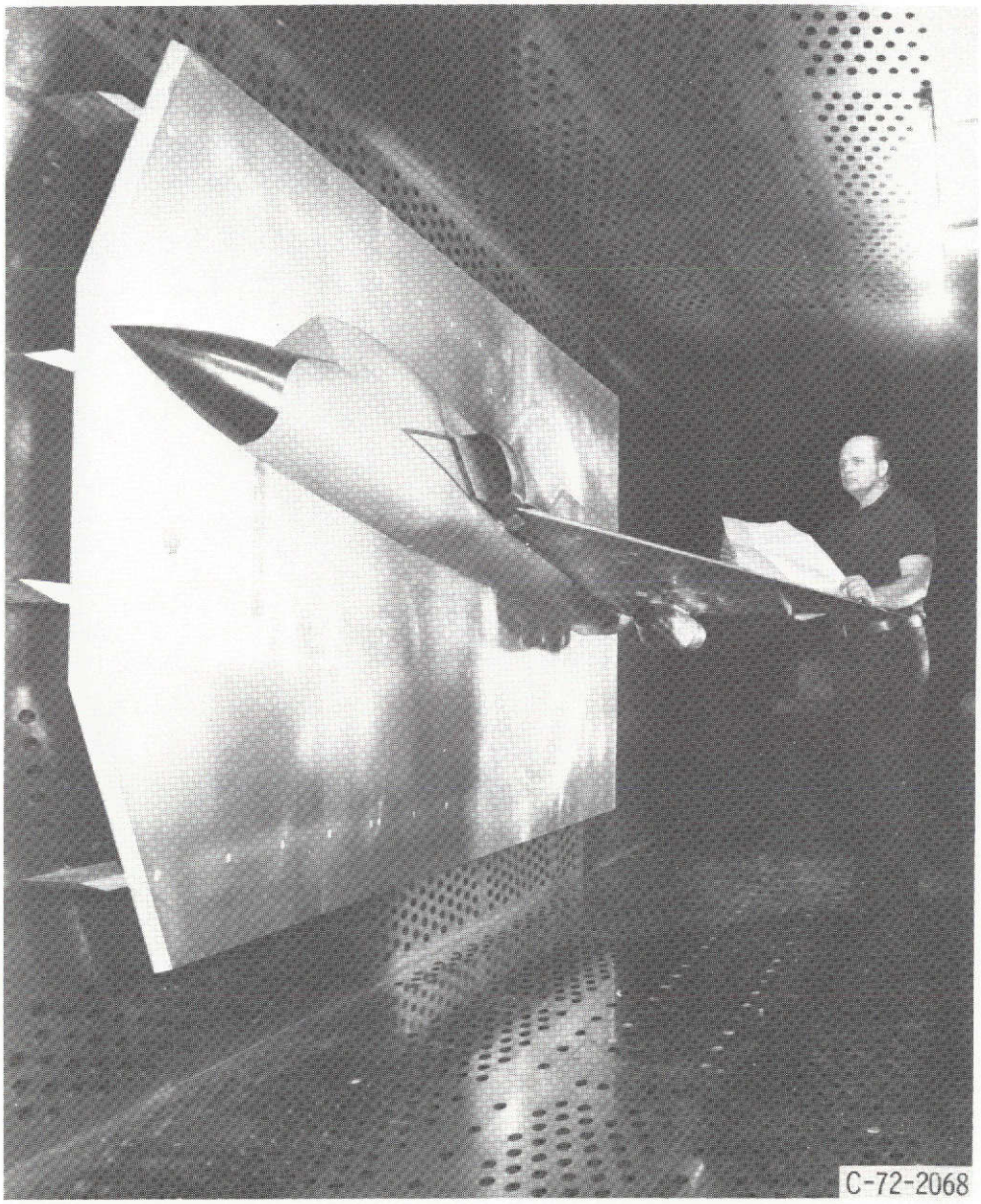

Figure 5. - 0.22 scale F-106 model in 8x6 tunnel.

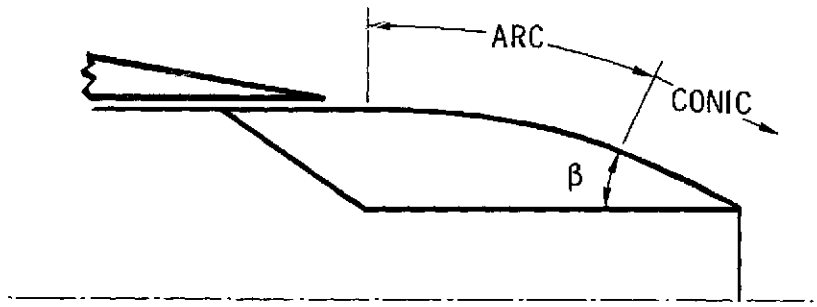

CIRCULAR ARC-CONIC

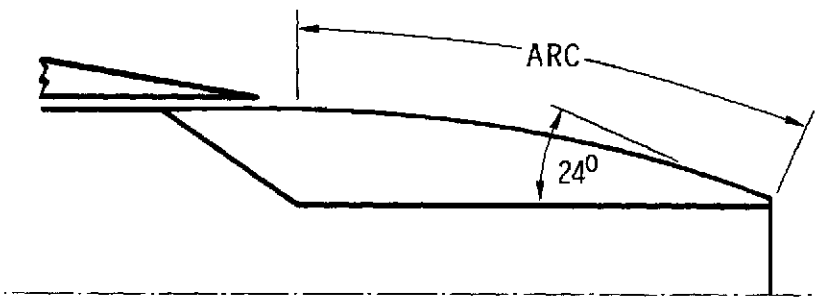

CIRCULAR ARC

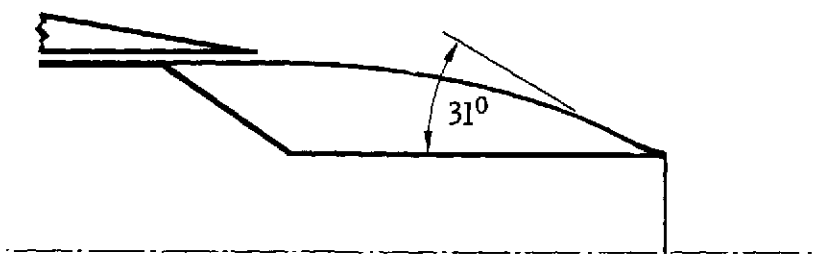

CONTOURED

Figure 6. - Schematic of boattail types.

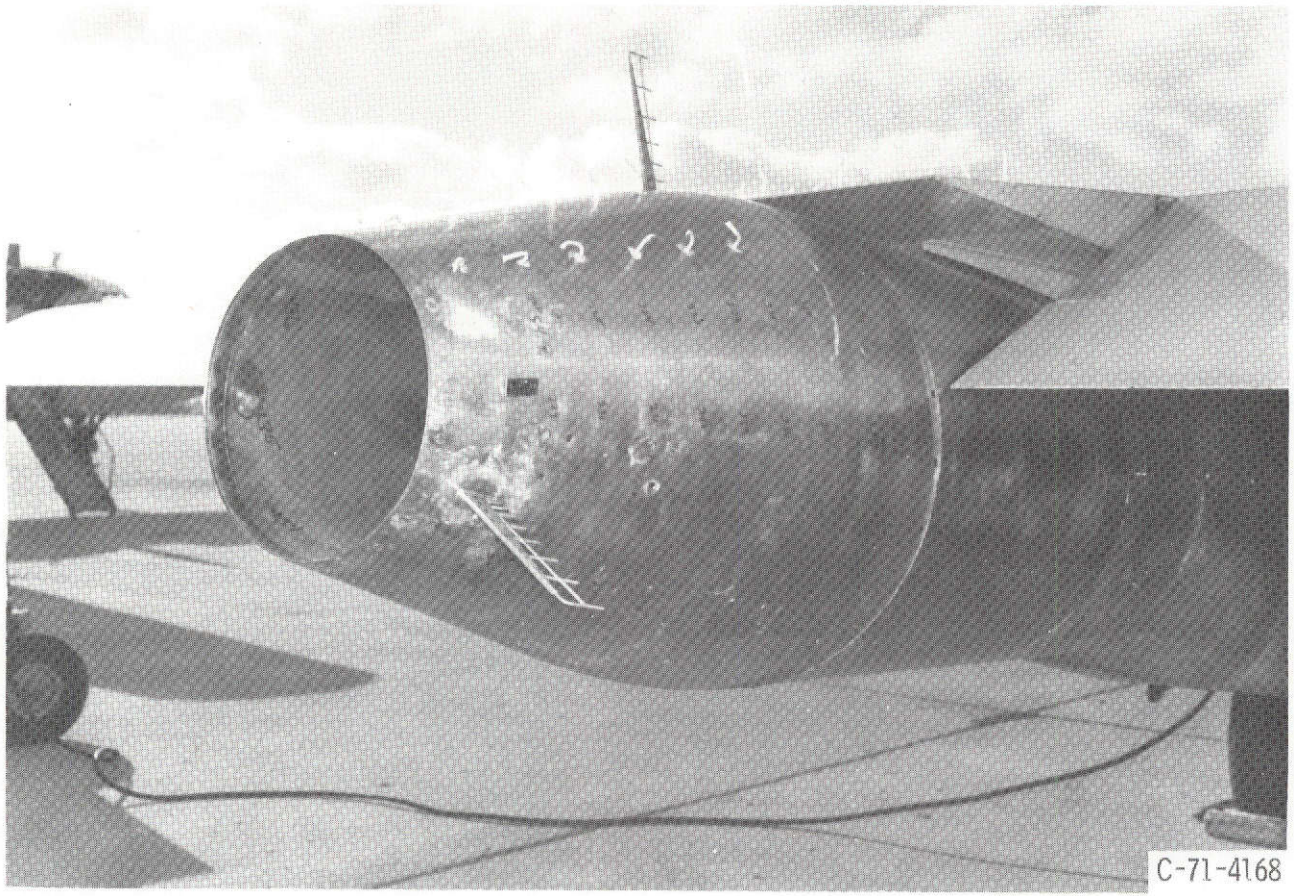

(a) Boattail nozzle 2516, radius ratio 0.25, boattail angle 16^{0}.

Figure 7. - Boattail nozzles.

(b) Boattail nozzle 2524, radius ratio 0.25, boattail angle 24°.

Figure 7. - Continued.

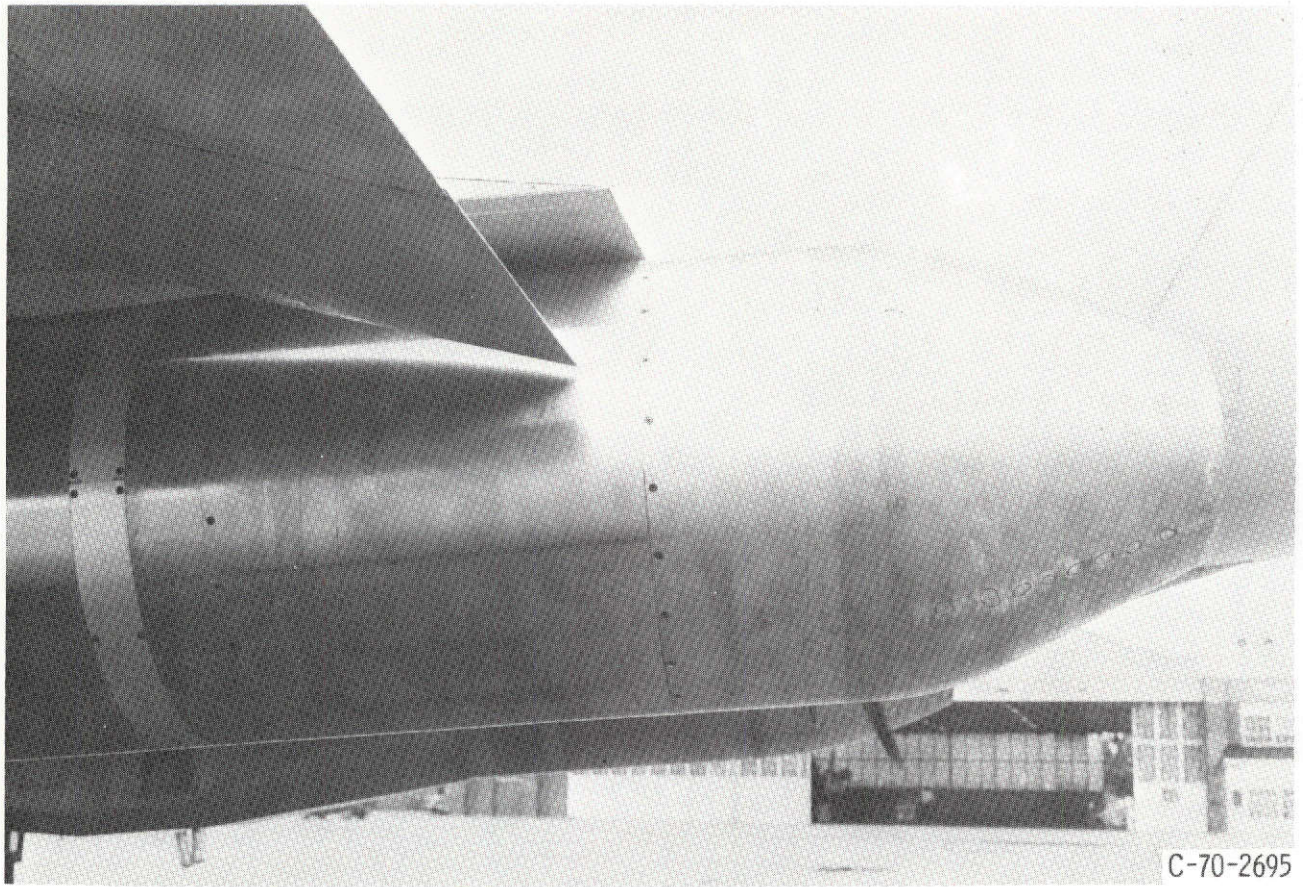

(c) Boattail nozzle 2524 Ex (extended), radius ratio 0.25, boattail angle 24^{0}.

Figure 7. - Continued.

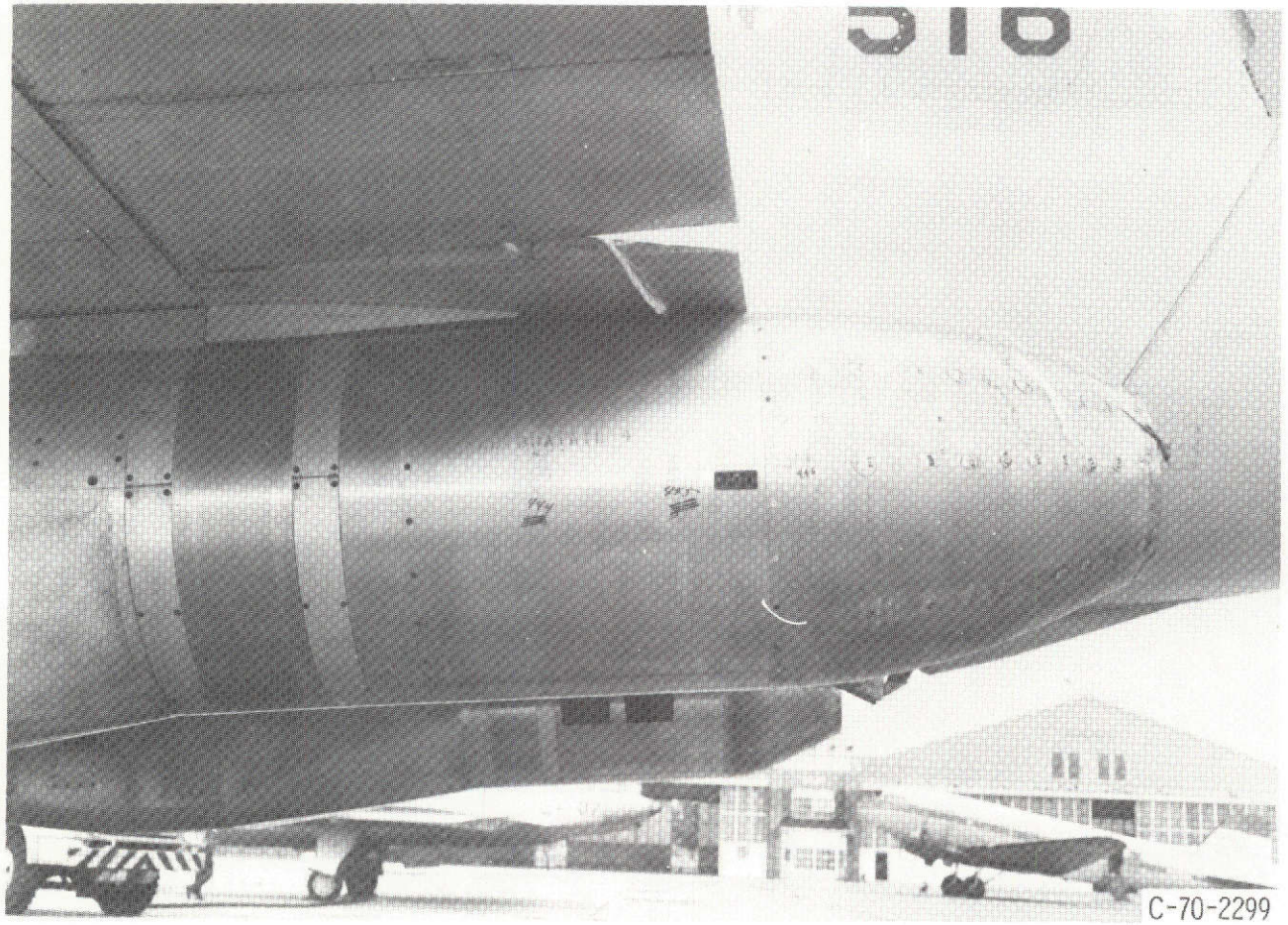

(d) Boattail nozzle 6524, radius ratio 0.65, boattail angle 24°.

Figure 7. - Continued.

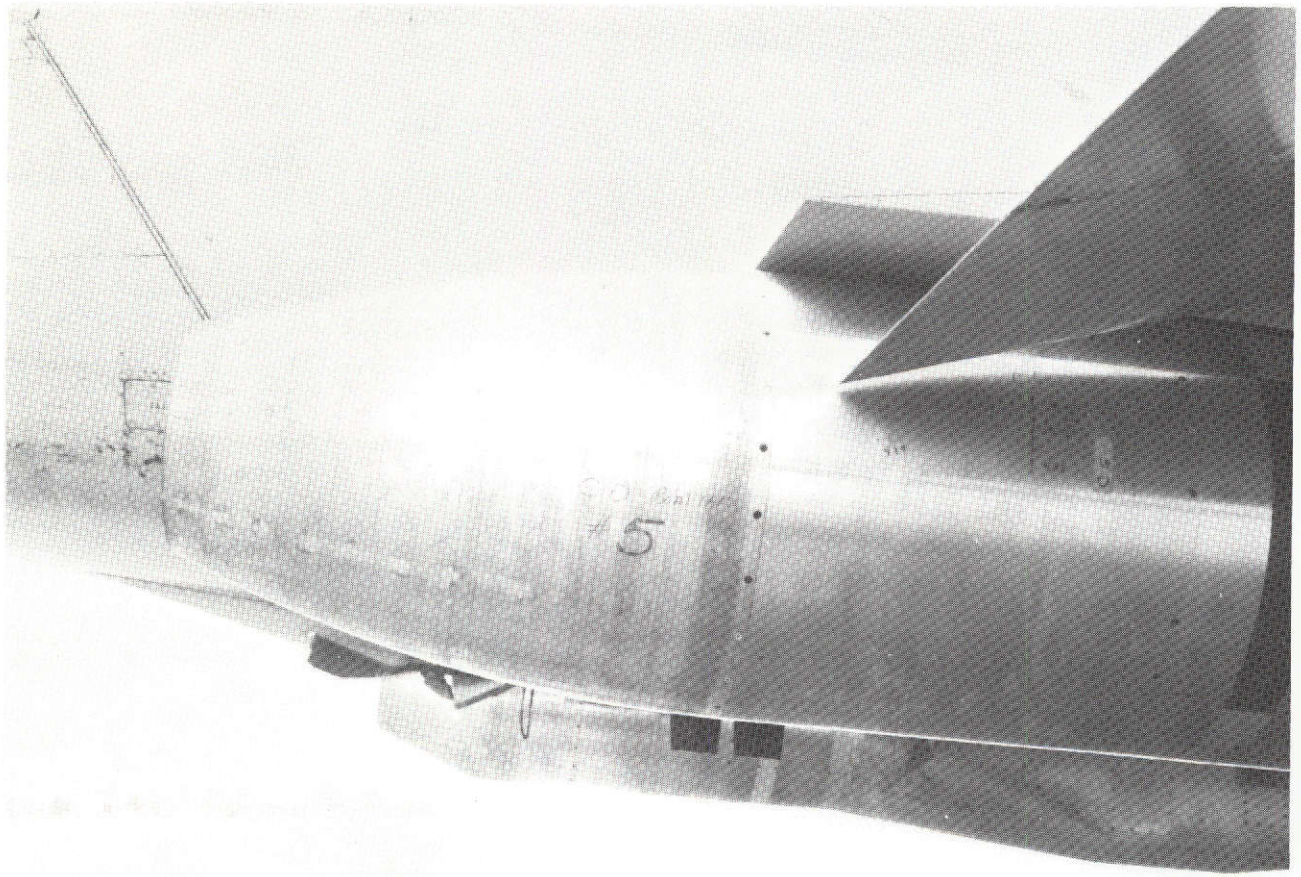

C-70-2692

(e) Boattail nozzle 10024, full circular arc, terminal boattail angle 24°.

Figure 7. - Continued.

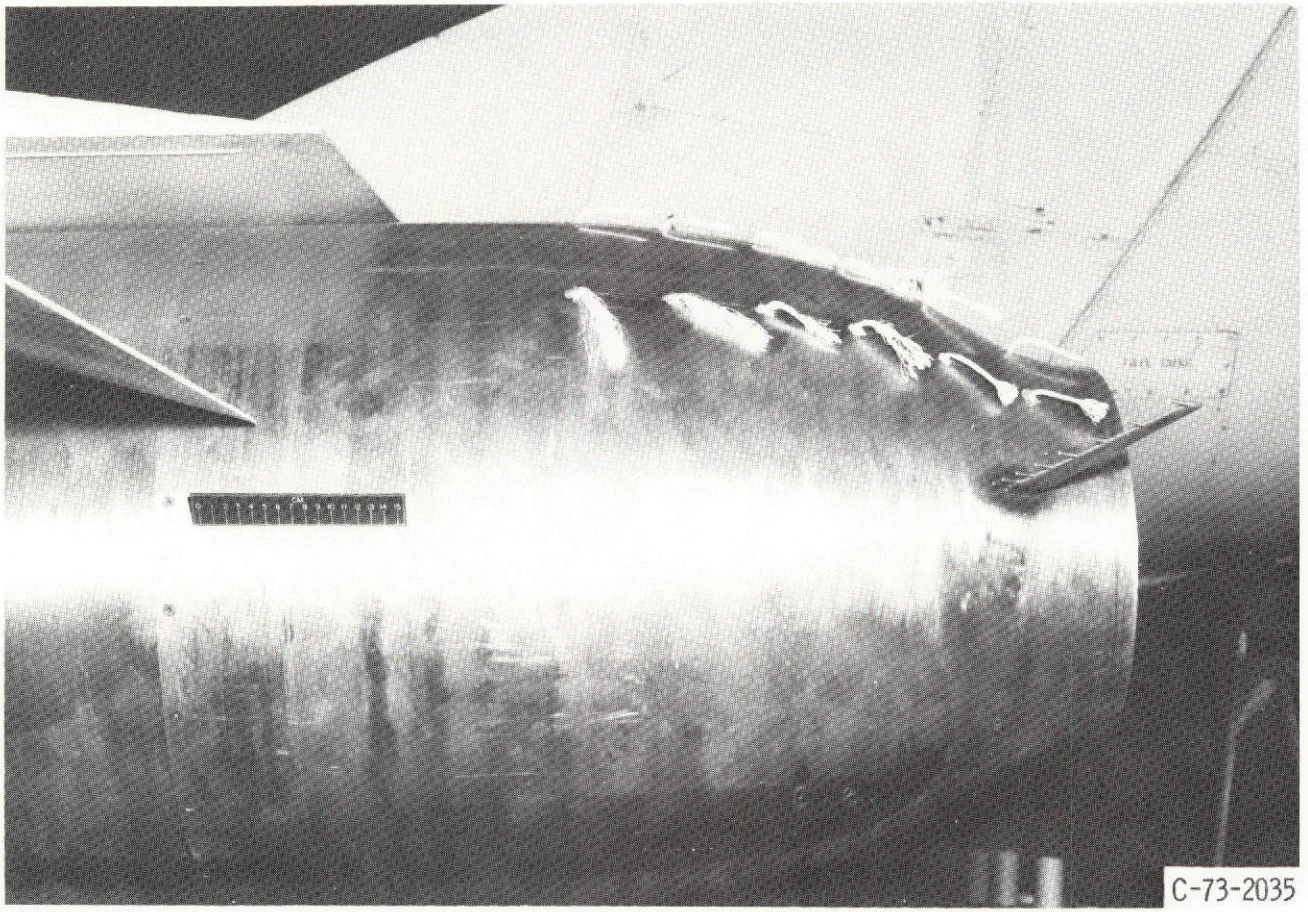

(f) Contoured boattail.

Figure 7. - Concluded.

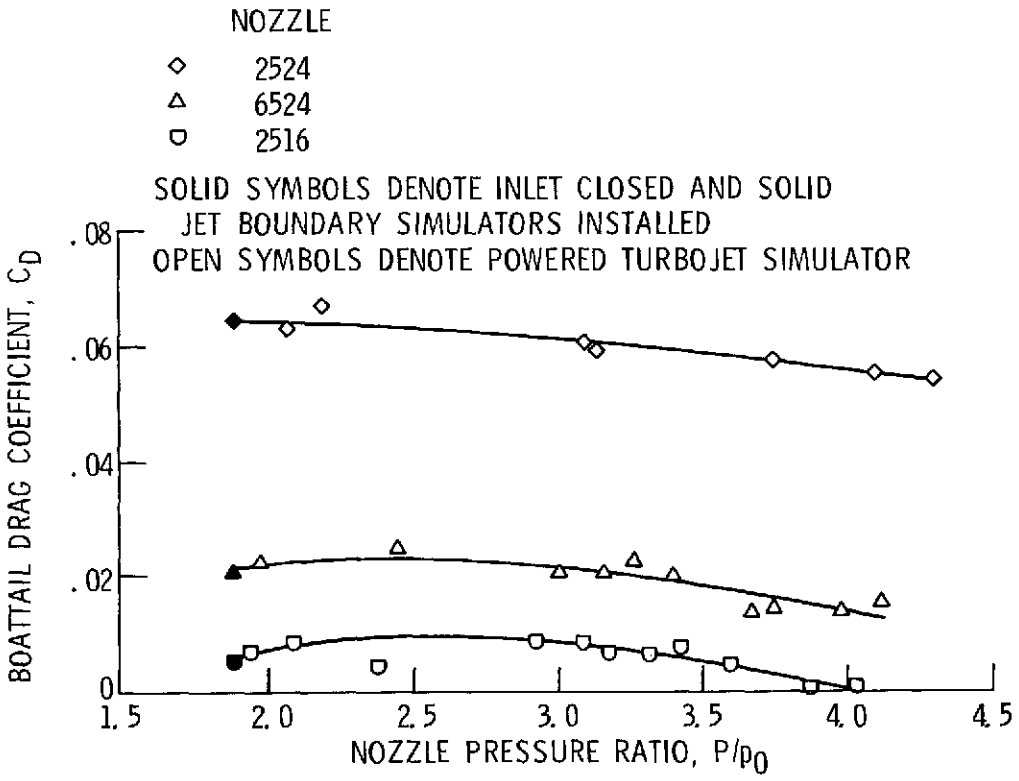

Figure 8. - Effect of pressure ratio on boattail drag on the 0.22 scale model; Mo, 0.9.

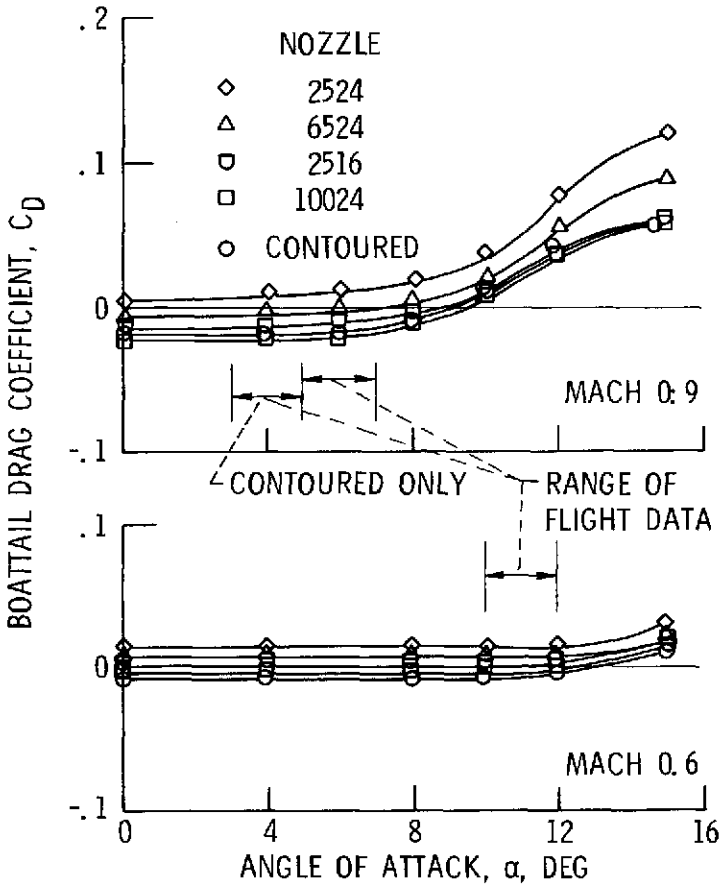

Figure 9. - Effect of angle of attack on boattail drag on the 0.05 scale F-106 model.

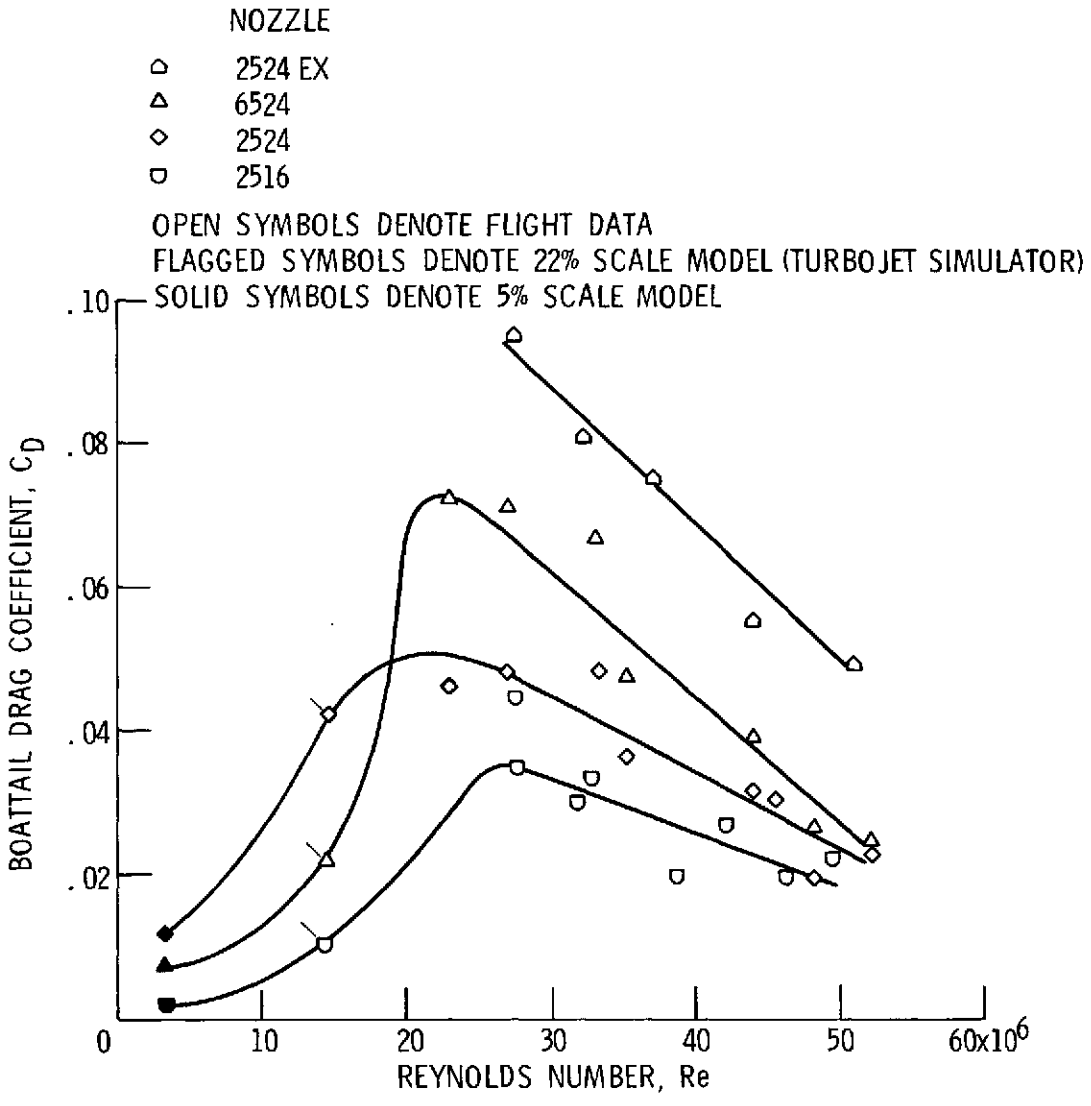

(a) MACH NUMBER, 0.6.

Figure 10. - Reynolds number effect on circular arc-conic boattails.

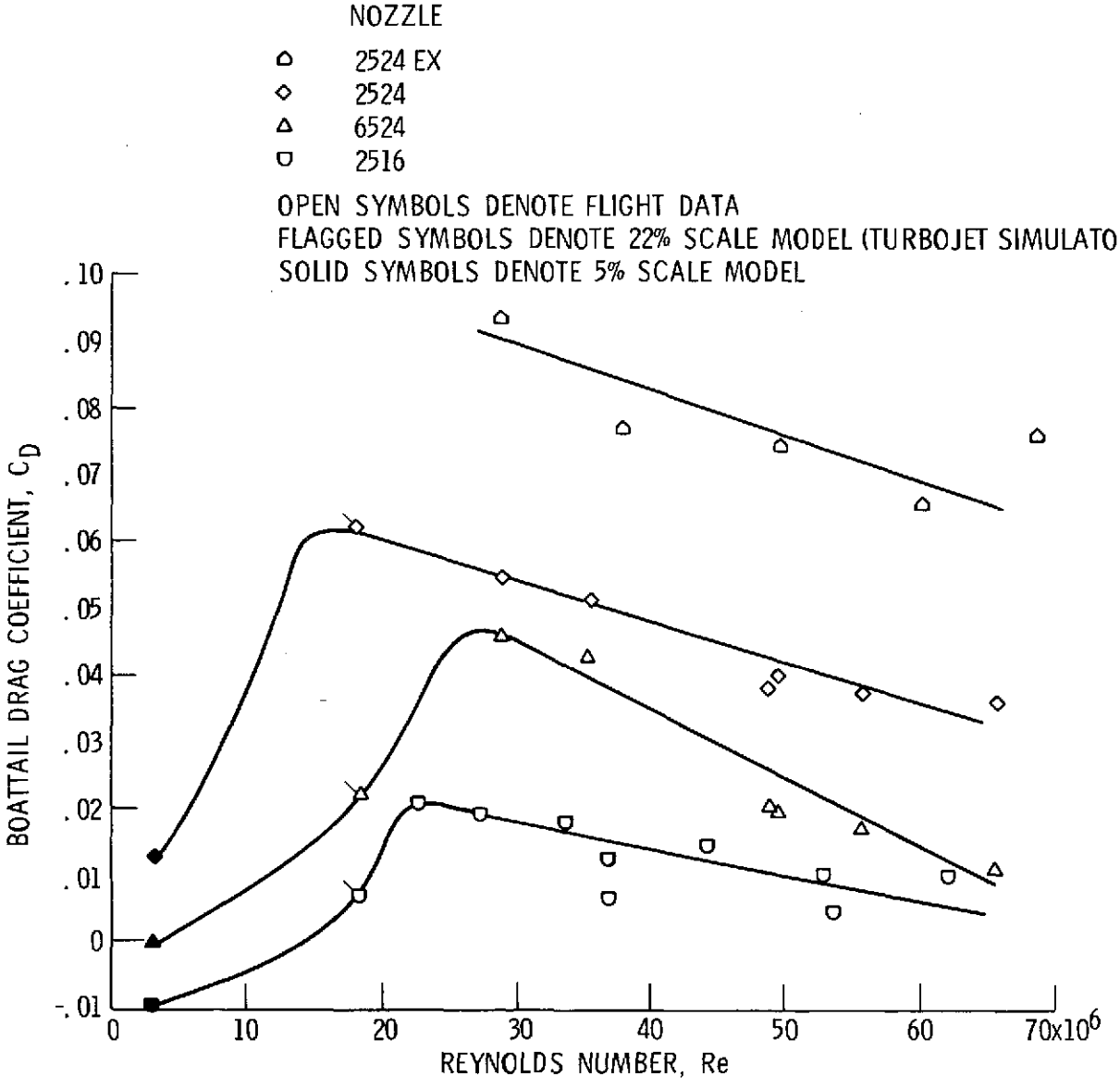

(b) MACH NUMBER, 0.9.

Figure 10. - Concluded.

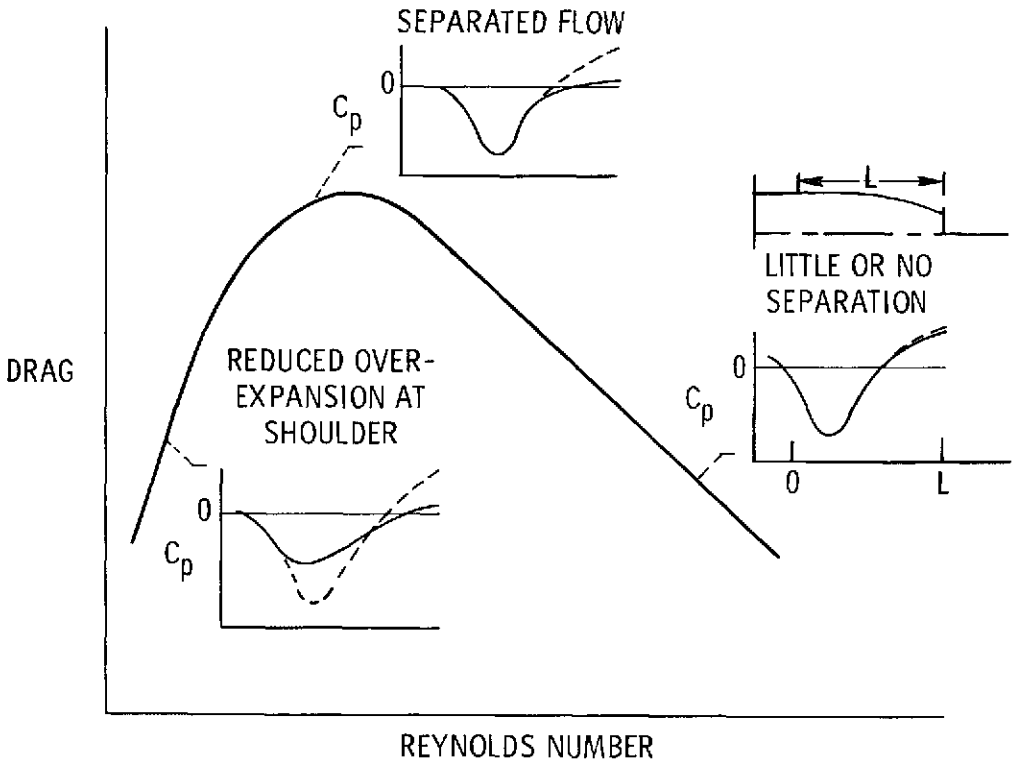

Figure 11. - Reynolds number effects on circular arc-conic boattails.

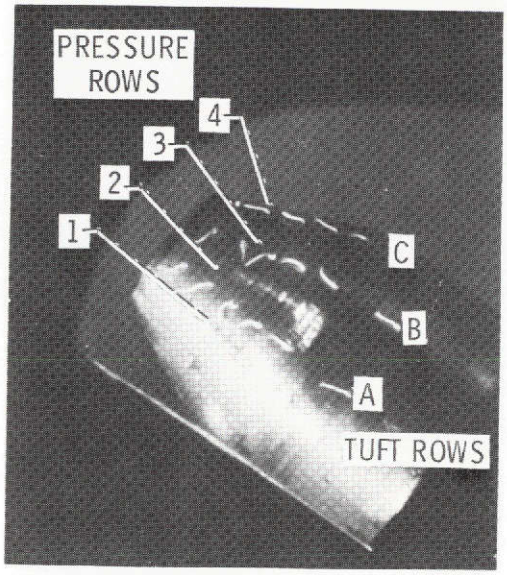

(a) TUFT PICTURE.

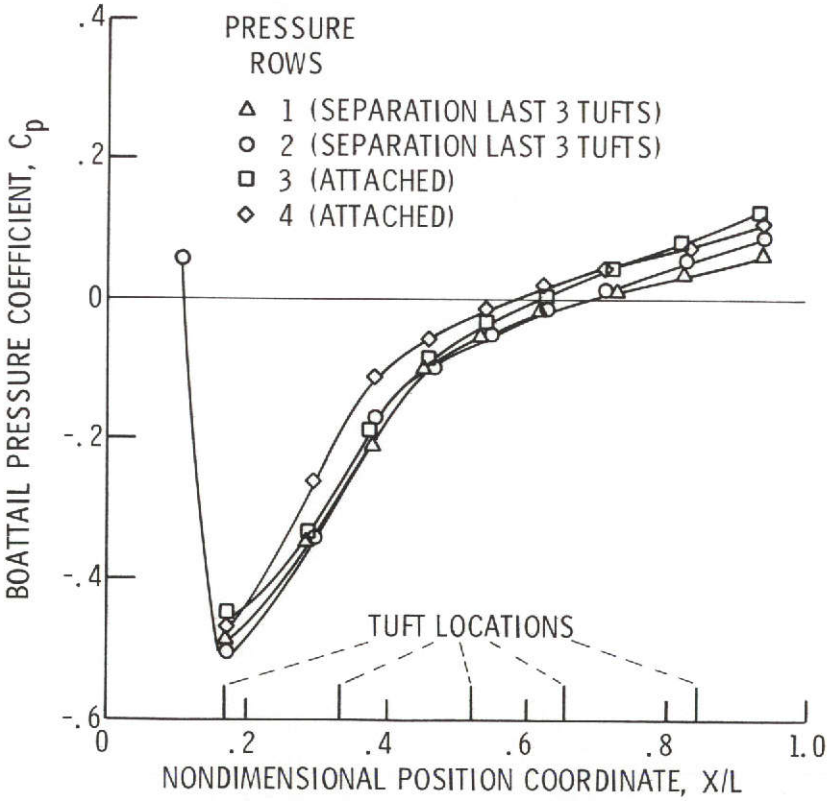

(b) PRESSURE DISTRIBUTION.

Figure 12. - Determination of separation. Nozzle 2524; Mo, 0.9; Re, 49.2×10^6.

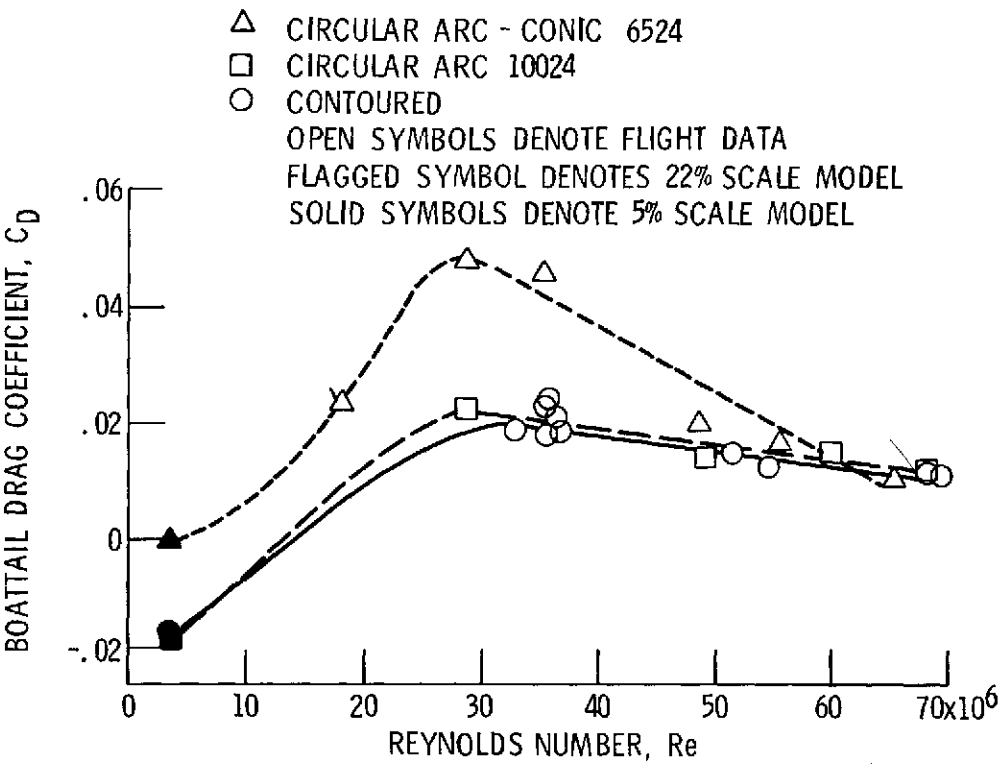

Figure 13. - Reynolds number effect on boattail geometries with attached and separated flows; M_0, =0.9; α, 4°.

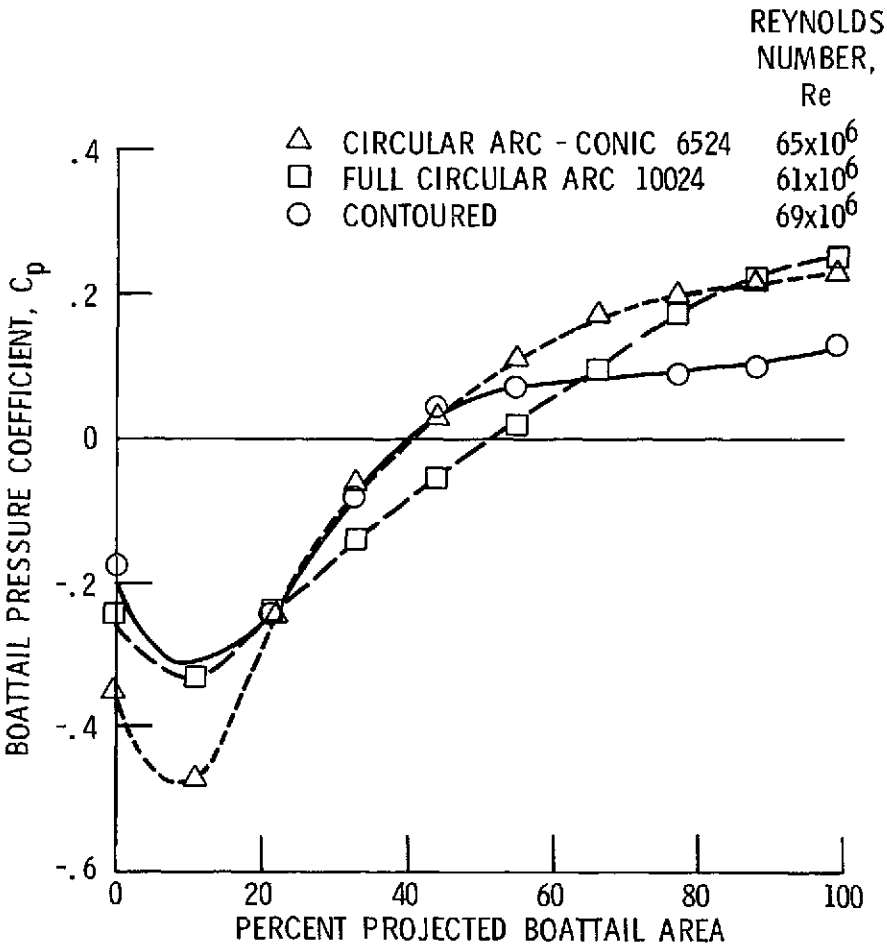

(a) HIGHEST FLIGHT REYNOLDS NUMBER.

Figure 14. - Pressure distributions on boattails with attached and separated flows. M_0, 0.9; 180° meridian angle.

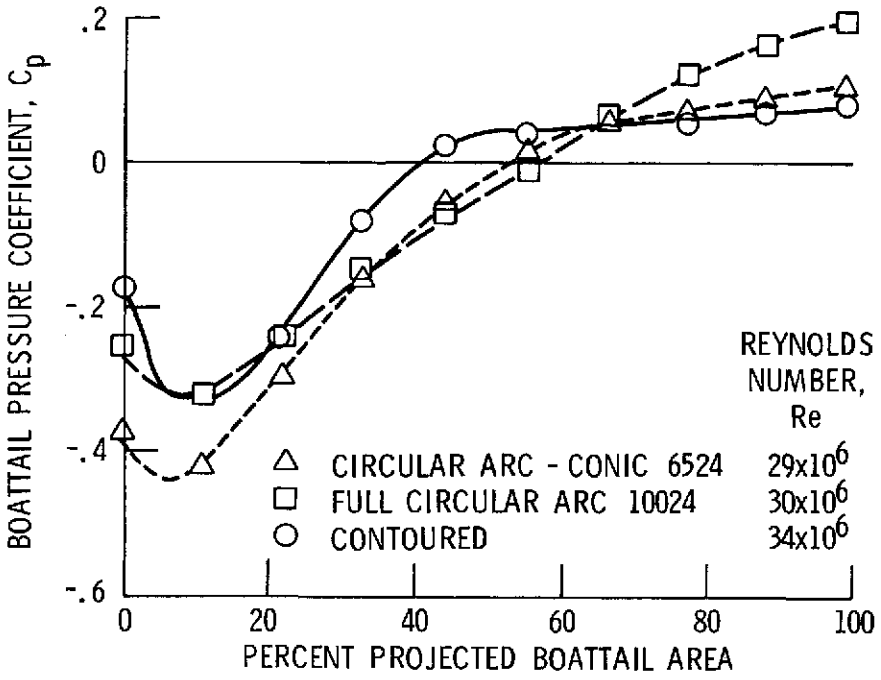

(b) LOWEST FLIGHT REYNOLDS NUMBER.

Figure 14. - Continued.

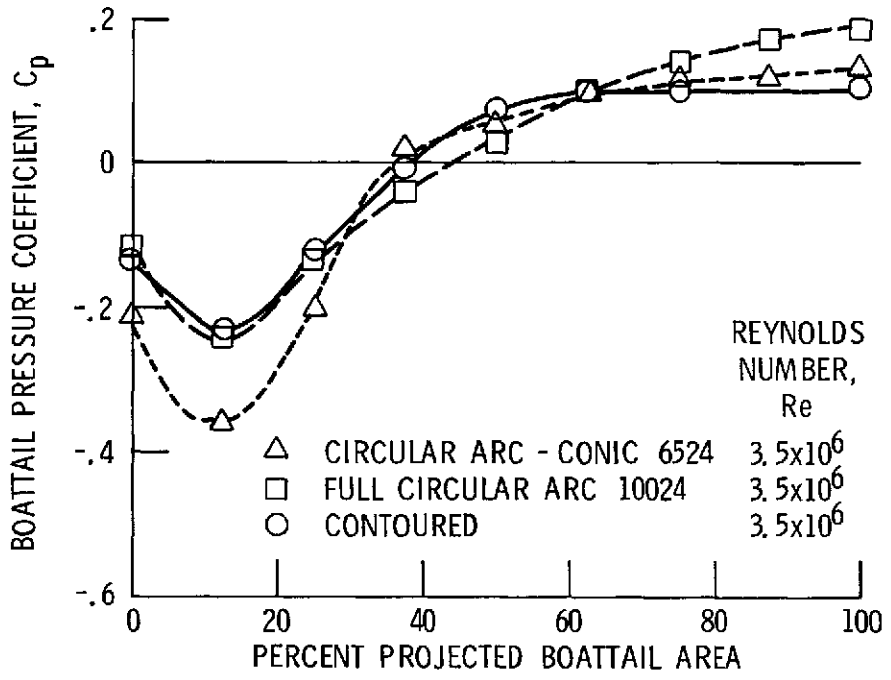

(c) 5 PERCENT SCALE REYNOLDS NUMBER.

Figure 14. - Concluded.